Analysis of ion dynamics and peak shapes for delayed extraction time-of-flight mass spectrometers

V. M. Collado, C. R. Ponciano, F. A. Fernandez-Lima,[a] and E. F. da Silveira[b]
Departamento de Física, Pontifícia Universidade Católica do Rio de Janeiro, Rua Marquês de São Vicente, 225, CP 38071 Rio de Janeiro 22452-970, Brazil

(Received 26 February 2002; accepted 14 January 2004; published online 24 May 2004)

The dependence of time-of-flight (TOF) peak shapes on time-dependent extraction electric fields is studied theoretically. Conditions for time focusing are analyzed both analytically and numerically for double-acceleration-region TOF spectrometers. Expressions for the spectrometer mass resolution and for the critical delay time are deduced. Effects due to a leakage field in the first acceleration region are shown to be relevant under certain conditions. TOF peak shape simulations for the delayed extraction method are performed for emitted ions presenting a Maxwellian initial energy distribution. Calculations are compared to experimental results of Cs^+ emission due to CsI laser ablation. © *2004 American Institute of Physics.* [DOI: 10.1063/1.1711161]

I. INTRODUCTION

The use of delayed extraction (DE) is commonplace in modern laser desorption time-of-flight (TOF) mass spectrometry (MS). Its capability to provide first-order correction for the initial energy distribution of emitted ions enabled increments in mass resolution and sensitivity and rendered the spectra less dependent on the laser intensity.

In this technique—introduced in 1955 by Wiley and McLaren as ''time-lag energy focusing'' [1]—ions are created and sequentially accelerated through two acceleration regions. In the first region, the electric field is turned on at a certain time after the ionization process took place; in the second one, the electric field is always constant. The correct choice of this delay time, as well as of the accelerating field magnitude, allows the initially slow ions—which spend a longer time in the extraction field—to receive enough additional energy to catch the initially fast ions (with the same mass) at the detector surface.

In 1983, Tabet and Cotter[2] were the first to point out the convenience of using Wiley and McLaren's technique[1] to improve laser desorption spectra as a method to measure ion initial energies. Ten years later, two groups[3,4] independently proposed the use of DE for improving spectrum quality in matrix assisted laser desorption ionization (MALDI), a technique introduced at that time to desorb intact ions of heavy biomolecules. As was already pointed out,[5,6] this important technical improvement turned MALDI into an attractive MS method for routine applications.

Several authors have made important contributions to understanding the fundamental aspects of DE. Barbacci *et al.*[7] examined the effects of ion kinetic energies and temporal variations in ion formation on peak widths, using both continuous and DE modes. In their work, they simulated the effects of ion initial position, initial velocity, delayed ion formation, and DE on arrival time distributions of MALDI formed ions. Though an analysis containing different graphs and a discussion were provided, there is still a lack of mathematical expressions that could be useful for achieving a better understanding of the particularities of DE.

Vestal and Juhasz[8] wrote one of the most complete reviews on the factors that affect resolution in modern TOF mass spectrometers. They developed a mathematical model of TOF analyzers which predicts flight time as a function of mass-to-charge ratio, initial velocity and position, applied voltages, and instrument geometry. Based on a series expansion of this exact result, a first-order approximation equation was derived, from which the focusing conditions and the limits on resolution could be determined for different instrument geometries and operating voltages. Instruments with one- and two-stage ion sources, with and without DE and a one-stage electrostatic mirror, were treated in their work.

The measurement of initial velocities of emitted ions using DE was previously addressed by Juhasz *et al.*[9] In their work, they show, both theoretically and experimentally, that the ion TOF changes linearly with extraction delay, making it possible to obtain the initial velocity of the ion from the slope of this dependence. Using this technique, Glückmann and Karas[10] performed a study of a broader list of matrices and analytes. A similar technique has been used in studies of ablation dynamics of different inorganic targets, such as carbon or cobalt.[11,12]

Recently, Berkenkamp *et al.*[13] measured the mean initial velocities of analyte and matrix ions produced by infrared laser ablation in MALDI experiments. DE measurements were also undertaken by Fournier *et al.*[14] to determine the dynamical effects involved in ion formation in standard MALDI. The last two works stress the significance, for ion dynamics under DE conditions, of the presence of field penetration in the ion source during the first stage prior to the application of the extraction voltage.

In this article, a contribution is given for the description

[a]Permanent address: Instituto Superior de Ciências y Tecnologia Nucleares, Havana, Cuba.
[b]Author to whom correspondence should be addressed; electronic mail: enio@vdg.fis.puc-rio.br

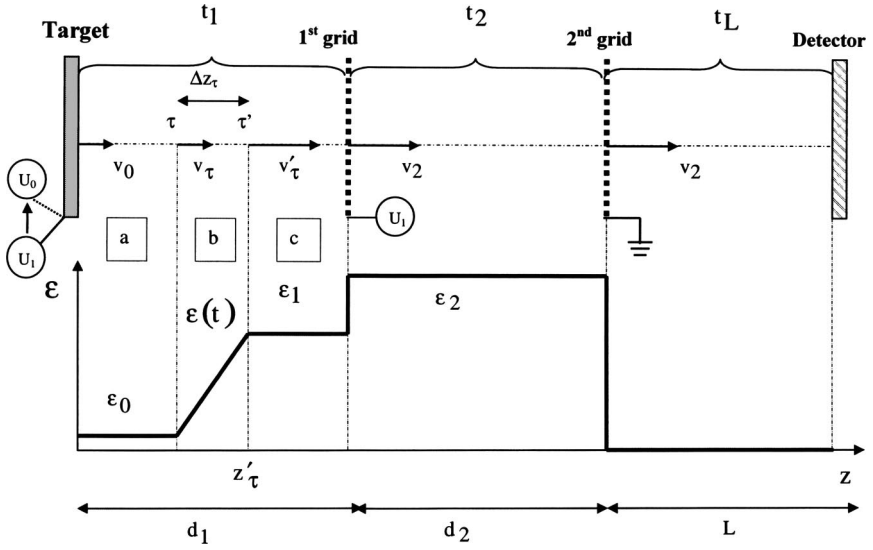

FIG. 1. Upper part: geometry of a three-region TOF spectrometer. t_1, t_2, t_L, d_1, d_2, and L are, respectively, the ion TOFs and the lengths relative to each region. The target potential increases from U_1 to U_0; the first- and second-grid potentials are U_1 and zero, respectively. Lower part: it is represented by the local electric field felt by the flying ion. In the first region, between the instants τ and $\tau' = \tau + \Delta\tau$, the field increases linearly. In the second region, the field is high, constant, and uniform; the third one is free field.

of the desorbed ion dynamics inside mass spectrometers, particularly when these ions are accelerated by external time-delayed electric fields which are modified by field penetration effects. A model for ion dynamics in a three-region TOF spectrometer is developed in Secs. II and III. In Sec. II, new (more general) TOF expressions are deduced for a two-stage ion source mass spectrometer under more realistic conditions, such as a finite time to switch on the field and leakage field effects due to the grids. Even though some approximations are used in the analytical approach, the obtained equations are quite helpful in understanding the influence of different parameters on ion TOF peak widths and the resolving power of TOF mass spectrometers equipped with DE. Considering the influence of leakage fields during ion extraction, a numerical step-by-step calculation is done instead of using a long analytical expression. In Sec. III, peak shape simulations are performed, assuming a Maxwellian distribution for the initial energies. Experimental data on CsI ablation are then compared to the model predictions.

Gridless instruments are interesting systems[15,16] in which DE can be also implemented. They require an analytical treatment more elaborate than the one discussed here and are out of the scope of the present work.

II. ION DYNAMICS MODEL FOR A THREE-REGION TIME-OF-FLIGHT SPECTROMETER

A. Time-of-flight equation for ramp-shape delayed extraction

For completeness, the general problem of determining TOFs is briefly reviewed in the Appendix. Based on these fundamentals, specific equations for a spectrometer configuration consisting of a double acceleration region and a field-free region (Fig. 1) can be obtained as follows. As three regions are separated by grids, an abrupt electric-field variation is considered to occur through the grid planes.

A variable sample potential $U_0(t)$ is assumed to have a ramp shape:

$$U_0(t) = U_1; \quad t < \tau, \tag{1a}$$

$$U_0(t) = U_1 + (U_0 - U_1)(t-\tau)/\Delta\tau; \quad \tau < t < \tau + \Delta\tau, \tag{1b}$$

$$U_0(t) = U_0; \quad t > \tau + \Delta\tau. \tag{1c}$$

The first acceleration region is divided into three subregions (a, b, and c), corresponding to each of the conditions given by Eq. (1). Velocities, time intervals, and electric fields in each situation are, respectively, defined in Fig. 1. In particular, the leakage field ε_0 is considered to be weak and constant in subregion a ($0 \leqslant t < \tau$) and negligible in the others; ε_1 is given by $(U_0 - U_1)/d_1$. Here, $\Delta\tau$ is the transient risetime associated with the application of the extraction pulse. Based on observations of the electrical signals, this transient is considered to have a ramp shape.

A useful reference time is $t_{G1}(\varepsilon_0, \nu_0)$, obtained from

$$d_1 = \nu_0 t_{G1}(\varepsilon_0, \nu_0) + \frac{1}{2}\frac{q\varepsilon_0}{m} t_{G1}^2(\varepsilon_0, \nu_0), \tag{2}$$

which is the ion TOF in the first region when the ion is emitted with initial velocity ν_0 and is accelerated only by the leakage field ε_0. Using Eqs. (1), (A5), and (A6), as well as the definitions

$$R = \frac{U_0 - U_1}{U_0} = \frac{\Delta U}{U_0}; \quad \nu_R = \sqrt{\frac{2q}{m}(U_0 - U_1)}, \tag{3}$$

and considering that the extraction voltage is turned on when ions are still far from the first grid [$\tau + \Delta\tau \leqslant t_{G1}(\varepsilon_0, \nu_0)$], one gets for the first region:

$$\nu_\tau = \nu_0 + \frac{q\varepsilon_0}{m}\tau \quad \text{and} \quad z_\tau = \nu_0\tau + \frac{1}{2}\frac{q\varepsilon_0}{m}\tau^2, \tag{4}$$

$$\nu'_\tau = \nu_\tau + \frac{R\nu_R^2}{4d_1}\Delta\tau \quad \text{and} \quad \Delta z_\tau = \nu_\tau \Delta\tau + \frac{R\nu_R^2}{12d_1}\Delta\tau^2, \tag{5}$$

$$\nu_1^2 = (\nu'_\tau)^2 + \frac{2q\varepsilon_1}{m}(d_1 - z_\tau - \Delta z_\tau), \tag{6}$$

$$t_1 = \tau + \Delta\tau + \frac{d_1 - z_\tau - \Delta z_\tau}{(\nu'_\tau + \nu_1)/2}. \tag{7}$$

The velocity at the exit of the second region is determined directly from Eq. (A5):

$$\nu_2^2 = \nu_1^2 + \frac{2q}{m}U_1, \tag{8}$$

and allows the calculation of TOFs in the second and third regions:

$$t_2 = \frac{d_2}{(\nu_1 + \nu_2)/2} \quad \text{and} \quad t_L = L/\nu_2. \tag{9}$$

The total TOF is finally given by

$$T(\tau, \nu_0) = t_1 + t_2 + t_L. \tag{10}$$

B. Negligible leakage field

An analytical expression for T can be obtained if the leakage field in the first acceleration region is neglected ($\varepsilon_0 = 0$). Taking also into account that the target–grid distance is much shorter than the free-field region length ($L \gg d_1$) and assuming that the inequality $\tau\nu_0 \ll d_1$ holds, expression (10) can be written as[17]

$$T(0,\nu_0) = T(0,0) + \tau + \left(w\tau - \frac{2d_1}{\nu_R}\right)\left(\frac{\nu_0}{\nu_R}\right) - \left(w\frac{d_1}{\nu_R} - w'\frac{\nu_R}{4d_1}\tau^2\right)\left(\frac{\nu_0}{\nu_R}\right)^2, \tag{11}$$

where

$$w = \frac{L}{2d_1}R\sqrt{R} + \frac{d_2}{d_1}\frac{R}{\sqrt{R}} - 1, \tag{12}$$

$$w' = \frac{L}{2d_1}3R^2\sqrt{R} + 2\frac{d_2}{d_1}\frac{\sqrt{R}}{1+\sqrt{R}}\left(R + \frac{1}{2}\frac{R^2+\sqrt{R}}{1+\sqrt{R}}\right) - 1, \tag{13}$$

and $T(0,0)$ is the ion TOF for $\tau = \nu_0 = 0$. There is a particular value of τ, called the critical delay τ_c, for which $T(\tau, \nu_0)$ becomes independent on small ν_0 variations ($\partial T/\partial\nu_0 = 0$) around a value, $\nu_0^{\max}$, corresponding to the maximum of the initial velocity distribution:

$$\tau_c = \frac{2d_1}{\nu_R}\left[\frac{1}{w} + \left(1 - \frac{w'}{w^3}\right)\frac{\nu_0^{\max}}{\nu_R}\right], \tag{14}$$

and the TOF of the time-focused ions is

$$T(\tau_c, \nu_0) = T(0,0) + \tau_c + \frac{d_1}{\nu_R}\frac{(1 - w'/w^3)^2}{w - w'}\left(\frac{\nu_0^{\max}}{\nu_R}\right)^2. \tag{15}$$

The last two expressions are particularly important, once they give the best delay [Eq. (14)] to obtain a time-focused peak of a given mass, as well as its position [Eq. (15)] in a TOF spectrum, for DE conditions.

As τ_c must be positive for physical reasons, it is promptly seen from Eq. (14) that w must also be positive when the ion initial velocity is very small compared to the velocity acquired during the acceleration in the first region ($\nu_0 \ll \nu_R$). Introducing this condition in Eq. (12) and observing that contributions of the second region are usually negligible, one gets that $R\sqrt{R}L > 2d_1$ is a necessary condition for the DE technique be efficient, that is to obtain a fully focused peak. For spectrometers in which $w' \ll w^3$, Eq. (14) reduces into the expression reported by Vestal *et al.*[9] The TOF peak width, ΔT, can be estimated from Eq. (15):

$$\Delta T \approx T(\tau_c, \nu_0^{\max}) - T(\tau_c, 0) = \frac{d_1}{\nu_R}\frac{(1 - w'/w^3)^2}{w - w'}\left(\frac{\nu_0^{\max}}{\nu_R}\right)^2. \tag{16}$$

The best mass resolving power of the spectrometer becomes, for $R\sqrt{R}L \gg 2d_1$:

$$P_m \equiv \frac{m}{\Delta m} = \frac{T(\tau_c, \nu_0^{\max})}{2\Delta T} \approx w\frac{q\varepsilon_1 L}{E_0^{\max}}\sqrt{\frac{\Delta U}{U_0}}. \tag{17}$$

C. Leakage field effects

If a grid separates regions with two different electric fields, the highest electric field "leaks" through the grid. This is a three-dimensional (3D) effect, in which intensity depends on the grid transmission coefficient and on the field variation at the interface of the regions. This effect is particularly noticeable around the first grid which separates the two acceleration regions: Before applying the extraction field, the first region should have zero field while the second region has a high acceleration field (~kV/mm).

The analytical solution for this electrostatic problem is difficult, so the potential distribution for both regions was simulated using SIMION 3D version 6.0. The target electrode and the first grid were considered at the same high potential ($U_1 = 280$ V), while the second grid was grounded ($U_2 = 0$); the target-first grid and grid–grid distances were $d_1 = 7.0$ mm and $d_2 = 20$ mm, respectively. The first grid was formed by nine meshes of $18.5 \times 18.5\ \mu\text{m}^2$ cross section wires, separated by 363 μm. These characteristics correspond to a grid having 70 wires/in. and 90% transmission coefficient. The electric field along the symmetry axis of the central mesh is presented in Fig. 2. One observes that field leakage exists all over the target-first grid region, remaining constant for the first half of it (ε_0) and rising steeply close to the grid. The greater the distance between the ion trajectory and symmetry axis, the larger the radial component of the leakage electric field close to the grid and the larger the angular deviation of the ion. This effect tends to decrease transmission and increase the ion TOF, broadening their spatial and TOF distributions.

Other SIMION simulations with several U_0 and U_1 potentials (which means different $\varepsilon_1 = (U_0 - U_1)/d_1$ and $\varepsilon_2 = U_1/d_2$ fields), different mesh geometries and other target–

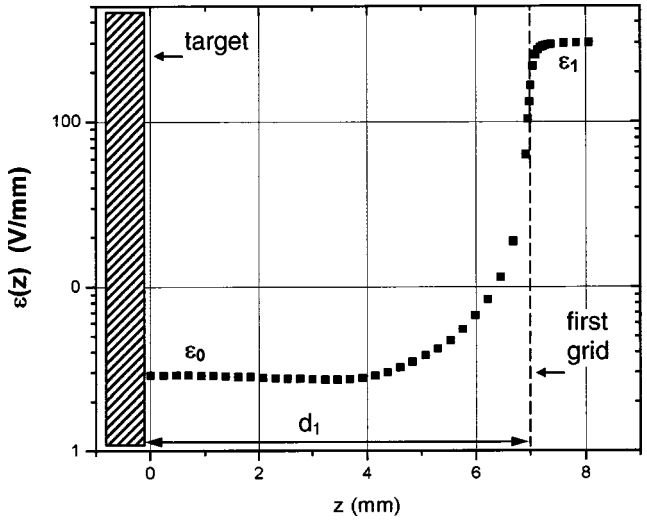

FIG. 2. SIMION 6.0 simulation of the leakage field in the first-acceleration region before extraction voltage is turned on. The *z* axis is perpendicular to the target and crosses the grid at the center of a hole. Note that the field is constant far from the grid.

grid distances revealed that the leakage field ε_0 is proportional to $(\varepsilon_2-\varepsilon_1)/d_1$ and depends on the grid transmission coefficient. So, for $U_0=U_1$, i.e., for $\varepsilon_1=0$:

$$\varepsilon_0=L_f\frac{\varepsilon_2}{d_1}. \tag{18}$$

The constant of proportionality L_f quantifies the thickness of a shell, inside which the leakage field is comparable to ε_2. For the 90% grid mentioned before, one gets $L_f\approx 65\ \mu$m. Considering $d_1=7$ mm, ε_0 turns out to be about 1% of the field in the second region. This leakage field, apparently negligible, is however high enough to increase, at half way of the grid, the ion kinetic energy (~eV, at the emission instant) by the amount

$$\Delta E_K=q\varepsilon_0\frac{d_1}{2}=\frac{L_f}{2d_2}qU_0, \tag{19}$$

which is about 0.5 eV for the current example. If leakage fields are not negligible, the use of Eqs. (1) or (7) yields ν_0 values which increase as τ increases.

It can be noted in Fig. 2 that the leakage field increases in the vicinity of the grid. Usually, such behavior does not sensibly affect the ion peak shape for three reasons: (i) After pulsing, ε_1 increases and, therefore, ε_0 decreases; (ii) the integral $\int\varepsilon(z).dz$ over this vicinity is small, so that the ion velocity does not change much; and (iii) ions with trajectories very close to the grid wires are deflected by intense transversal forces and may be not detected. Two other possible approaches to reduce the leakage influence on the ion's TOF should be mentioned:

(1) The application of a negative, weak, and permanent external field can minimize the leakage field.[9,14]
(2) The first and second grids of the target are initially kept at the same potential [so, $\varepsilon(z)=0$ strictly]. Then, at $t=\tau$, both fields ε_1 and ε_2 are pulsed.

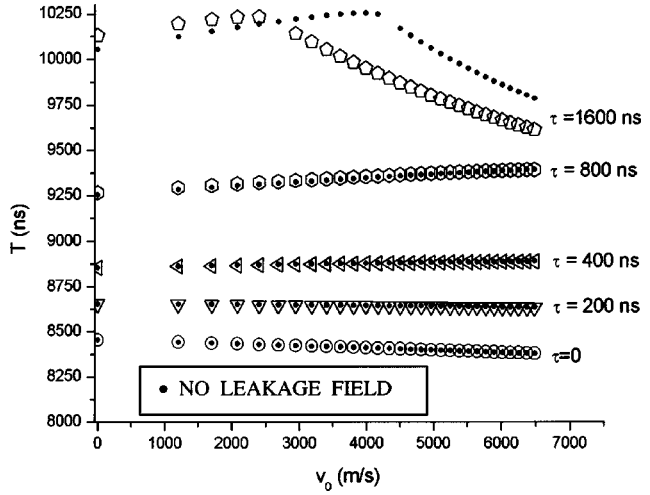

FIG. 3. Effect of the leakage field on the ion TOF as a function of ν_0 and for some values of τ. The black and open symbols correspond, respectively, to zero and $\varepsilon_0=100$ V/cm leakage field, which is caused by the first-grid openings.

D. Model properties

The main characteristics of the leakage-free model can be deduced from Eqs. (11)–(15) and from the numerical calculations are presented in Figs. 3–5:

(a) If $\tau\leqslant t_{G1}(\varepsilon_0,\nu_0)$, the TOF $T(\tau,\nu_0)$ is roughly linear on τ, for a given ν_0.
(b) For a fixed τ, $T(\tau,\nu_0)$ presents a smooth parabolic dependence on ν_0. The value of its maximum is given by Eq. (15) and occurs at $\nu_0=\nu_0^{\max}$.
(c) If $\tau>t_{G1}(\varepsilon_0,\nu_0)$, $T(\tau,\nu_0)$ becomes constant: The ion is already in the second acceleration region when the extraction field is applied, so that its movement can no longer be altered by a variable field in the first region. In this case, the ion initial velocity is directly determined by Eq. (2).
(d) For a particular value of τ, called the critical delay (τ_c), there is time focusing, which means

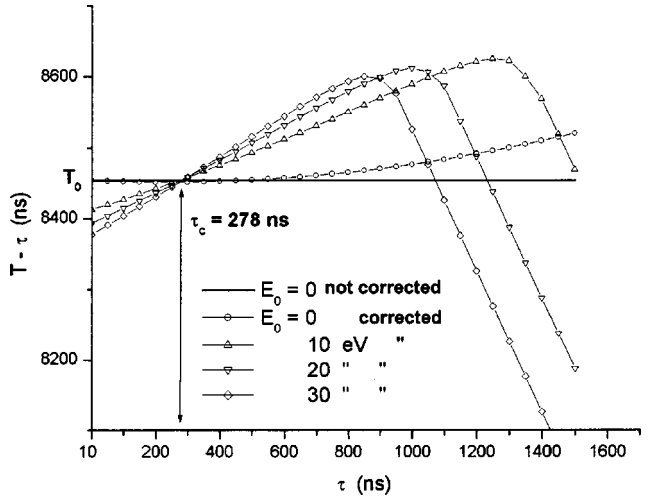

FIG. 4. $T-\tau$ versus τ. T is the ion TOF and τ is the time interval during which no extraction field is applied. In the inset, the existence of time-focusing aberration is shown.

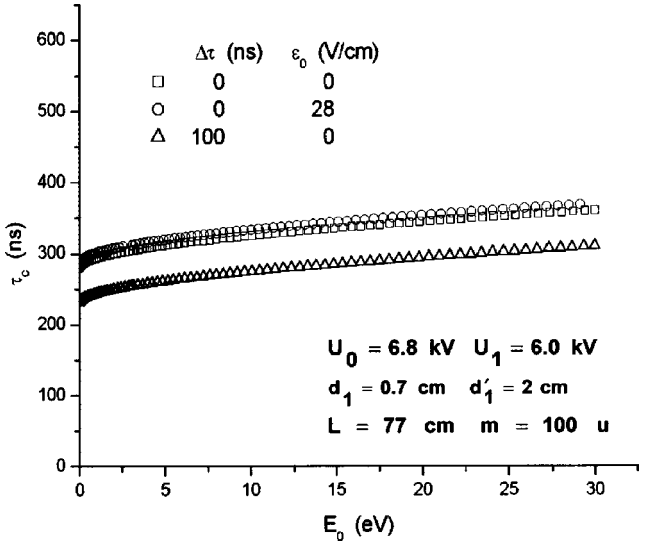

FIG. 5. Aberration in the time-focusing: τ_c depends on E_0. Calculations have been done for zero- (open squares) and for nonzero-leakage field (open circles); effects due to $\Delta\tau=100$ ns are represented by open triangles.

$\partial T(\tau_c,\nu_0)/\partial\nu_0\approx 0$. The τ_c value is very important for mass spectrometry because it gives the conditions of maximum time resolving power.[1,8] For mechanism analysis purposes, it assists in the accurate determination of $T(0,0)$ and allows more accurate initial velocity measurements.

(e) If $\nu_0/\nu_R \ll 1$, the τ_c dependence on ν_0 is linear:

$$\tau_c(\nu_0)\approx\tau_c(0)\left[1+\left(w-\frac{w'}{w^2}\right)\frac{\nu_0}{\nu_R}\right]. \tag{20}$$

(f) The main effect of the leakage field ε_0 is to increase the ion velocity before the extraction, simulating a higher value of ν_0, which is the reason why the τ_c for this situation should be accordingly higher.

(g) Equation (11) is the fundamental expression for the initial velocity measurement based on the DE technique. Considering $\nu_0 \ll \nu_R$, the first-order term indicates that as τ increases, the slope of $T-\tau$ changes with the slope $(w/\nu_R)\nu_0$. For such measurements, the quantity w/ν_R should be high in order to observe large $T-\tau$ shifts.

E. Time-lag energy focusing by delayed extraction

Simulations of ion dynamics were performed using several codes written in LABVIEW 5.1 (National Instruments) following the approach illustrated in the Appendix.

Considering $m=133\,u$, Fig. 3 illustrates $T(\tau,\nu_0)$ as a function of ν_0, for $\varepsilon_0=0$ and for $\varepsilon_0=100$ V/cm. The spectrometer configuration is $d_1=0.70$ cm, $d_2=2.0$ cm, $L=77$ cm, $U_0=6.80$ kV, $U_1=6.00$ kV, and $\Delta\tau=100$ ns, implying that $R=0.133$, $w=1.47$, $w'=0.149$, $\nu_R=0.00393$ cm/ns, and $\tau_c(\nu_0=0)=278$ ns. It can be seen in Fig. 3 that the slope $dT/d\nu_0$ exchanges sign at $\tau=\tau_c$. For a large enough τ (1600 ns in the example), the ion reaches the first grid before the extraction field is applied, so that T decreases as ν_0 increases. Equation (11) shows that T is trivially increased by τ when the extraction field is delayed by this quantity, therefore it is more convenient to analyze time-focusing effects in a $T-\tau$ plot. Such time-lag energy focusing is illustrated in Fig. 4, which shows $T-\tau$ as a function of τ for some values of the initial energy $E_0=m\nu_0^2/2$, considering $\varepsilon_0=0$ ("not corrected" curve) or $\varepsilon_0=28$ V/cm ("corrected" curves). For small values of τ, a linear dependence occurs; the slope increases as E_0 increases because $w>0$. At $\tau=\tau_c$, there is time focusing. For $\tau>t_{G1}$ (for each corresponding E_0), T becomes constant and independent on τ, so that $T-\tau$ decreases. Over a wide emission energy range, the ions arrive almost simultaneously on the detector if the delay is τ_c. In the inset of Fig. 4, a simulation with smaller steps on E_0 shows the existence of time-focusing aberrations, i.e., a τ_c dependence on E_0.

Figure 5 shows, for another spectrometer drift length ($L=77$ cm), the sensitivity of the τ_c dependence on E_0 [in fact, Eq. (14) shows that it has a linear dependence on $E_0^{1/2}$] and also how this time-focusing aberration is affected by the leakage and by the existence of a ramp shape extraction pulse. Three situations have been considered: (i) $\varepsilon_0=\Delta\tau=0$, (ii) $\varepsilon_0=28$ V/cm and $\Delta\tau=100$ ns, and (iii) $\varepsilon_0=0$ and $\Delta\tau=100$ ns. The $\varepsilon_0\neq 0$ correction implies a slight increase of the τ_c value. On the other hand, the $\Delta\tau$ value has the effect of shifting down τ_c by $\Delta\tau/2$, about 20 ns in the simulation.

III. SIMULATIONS OF TIME-OF-FLIGHT ION PEAK SHAPES

To observe how the TOF peak shape depends on τ, simulations were done assuming a Maxwellian distribution for the initial energies E_0:

$$\frac{dN}{dE_0}=AE_0e^{-E_0/k\Theta}=A\frac{1}{2}m\nu_0^2e^{-m\nu_0^2/2k\Theta}, \tag{21}$$

where the parameter Θ may be interpreted as the average temperature of the ejecta.

The peak shape, without any "walk" from the electronic equipment (i.e., the peak dispersion is uniquely due to the initial velocity spread), is the TOF distribution defined by

$$\frac{dN}{dT}=\frac{dN}{dE_0}\frac{dE_0}{dT}, \tag{22}$$

where dN/dE_0 is given by Eq. (21), $dE_0/dT=m\nu_0/(dT/d\nu_0)$ and $dT/d\nu_0$ can be determined by derivation of Eq. (10).

Simulations for $\Theta=5000$ K (i.e., $k\Theta=0.43$ eV) and for $\varepsilon_0=0$ are presented in Fig. 6 for five values of τ (namely: 0, $\tau_c/2$, τ_c, $t_1/2$, and t_1). In the inset of Fig. 6, the initial Maxwellian energy distribution for this temperature is displayed. One sees that as τ increases, the peak moves to longer TOF values, shrinks continuously up to $\tau=\tau_c$, folds into itself, and then spreads out. For such transformations, it is important to mention that the detection efficiency is assumed to be constant, so that the area under the peaks—representing the total number of emitted ions of that species—also remains constant. When $\tau\approx t_{G1}$, the ions reach the first acceleration grid and variations on ε_1 can no longer alter their TOF. The peak shape becomes independent on τ, if $\tau>t_{G1}$.

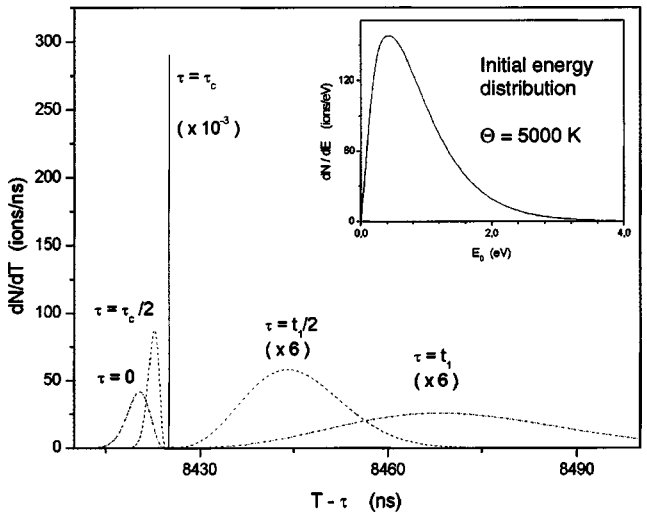

FIG. 6. TOF peak shapes (dN/dT vs $T-\tau$) for different τ. Note the peak inversion at the time-focusing condition $\tau=\tau_c$: For $\tau>\tau_c$, low E_0 ions reach the detector before the higher E_0 ones. Events corresponding to $E_0=0$ have a constant $T-\tau$ value. Field leakage effects are not taken into account.

As presented in Fig. 7, the effect of the leakage field on the TOF peak shape can be analyzed by plotting the peak limits (abscise) as a function of τ (ordinate). At right-hand side of Fig. 7, the two dotted lines show the peak narrowing in the absence of leakage field: At $\tau=\tau_c$, the peak width vanishes completely (neglecting the time-focusing aberrations). At the left-hand side of Fig. 7, considering a leakage field of $\varepsilon_0=57$ V/cm, the gray region represents the peak position as τ increases. Up to $\tau\approx1000$ ns, a peak narrowing is observed; for higher τ values, the peak spreads out. The leakage field has the effect of quickly moving apart the particles of different initial velocities, deteriorating the time-focusing property of the delayed extraction method.

In Fig. 8(a), a TOF spectrum simulation for Cs^+ ions is performed to show how the peak position and shape evolve

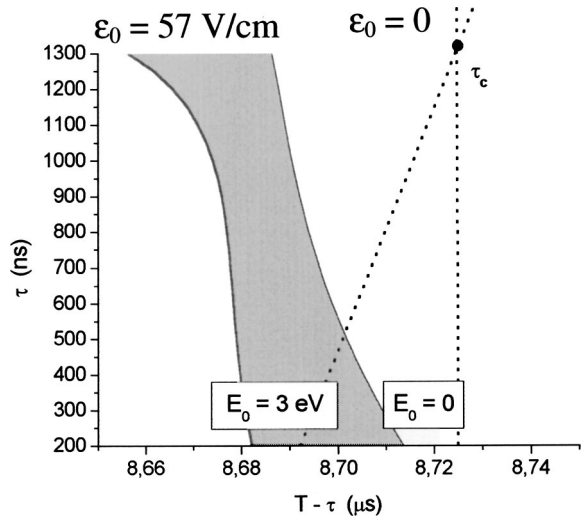

FIG. 7. TOF peak boundaries (abscissa shifted by τ) for several extraction field delays (τ). Initial energies of all desorbed ions are assumed to lay in the 0–3 eV range. The dotted lines correspond to zero-leakage field; for $\tau=\tau_c\approx1300$ ns, the peak width vanishes. If a leakage field $\varepsilon_0=57$ V/cm exists, the peak width (in gray) goes into a minimum at $\tau\approx1000$ ns.

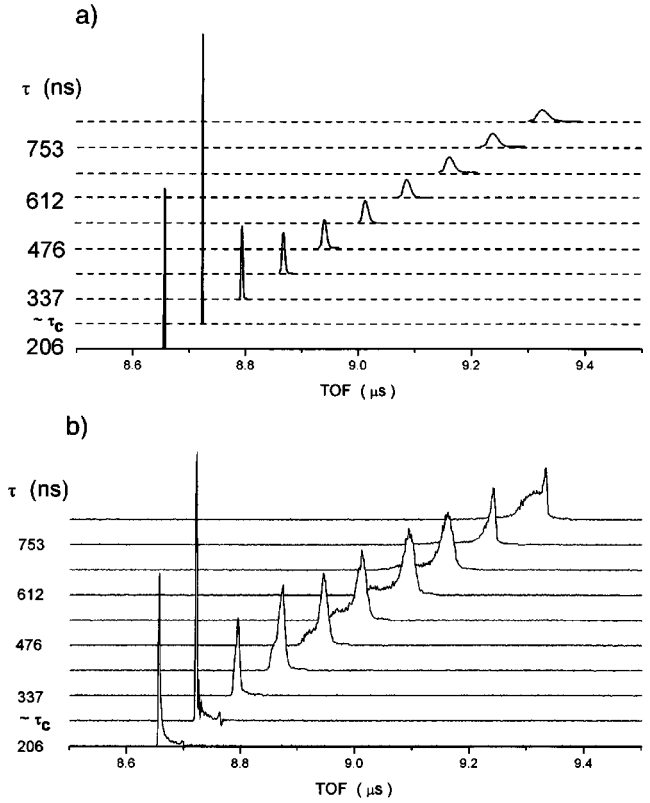

FIG. 8. Position and shape of $m=133u$ TOF peaks as τ varies from 200 to 800 ns. (a) Simulation: Ion initial energies range from 0 to 10 eV. Leakage field intensity is considered to be $\varepsilon_0=28$ V/cm. (b) Experiment: The narrowest (and highest) TOF peak is observed for $\tau\sim278$ ns, value close to the one predicted by simulations.

as τ increases. Initial energies in the 0–10 eV range and a $\varepsilon_0=28$ V/cm leakage field are assumed in these calculations. The main behavior of the peak position is its shift of $\sim\tau$ toward longer TOFs when τ increases [as imposed by Eqs. (7) or (11)]. Note the peak flipping and the highest detection sensitivity at a τ near τ_c. A new flipping occurs (not shown in the figure) when τ becomes comparable to t_{G1}, a situation in which the extraction field is applied while the ions are crossing the first grid. Figure 8(b) presents experimental results which are discussed in Sec. V.

IV. EXPERIMENT

All experiments were carried out in a homemade two-stage ion source linear TOF mass spectrometer equipped with a DE system. The 337 nm radiation from a nitrogen laser (VSL-337-ND-S, Laser Science Inc., Franklin, MA) was brought into focus on the target with a 30° incidence angle after passing through a variable density neutral attenuator from Oriel (Stratford, CT).

The ion extraction region is composed of two stages, each one ended by a 90% transmission electroformed nickel grid (Buckbee Mears, St. Paul, MN) having 70 wires/in. Distances from the target to the first grid (d_1) and between the first and second grids (d_2) are, respectively, 7.0 ± 0.1 and 20.0 ± 0.1 mm. The drift tube L is 276.5 ± 0.1 mm. The target is mounted on a precision $X-Y-Z$ manipulator. Two high stability power supplies (HCN 14-20000 and HCN 35-

30000, F.u.G. Elektronik GmbH, Rosenheim, Germany) were used to bias the target holder and the first grid ($U_0 = 6.80$ kV and $U_1 = 6.00$ kV). A pair of microchannel plates mounted in a chevron configuration was used as ion detector.

The DE system was based in a high-voltage switch HTS300 (Behlke Electronics, Kronberg, Germany). A high-voltage positive pulse was applied to the target electrode. A rise time of about 110 ns was observed, and the delay time between laser and extraction pulses was varied from 200 ns up to 1200 ns using three delay boxes (DB463, EG&G ORTEC, Oak Ridge, TN).

CsI (99.9% purity, Merck, Darmstadt, Germany) polycrystalline films, grown over stainless-steel substrates by deposition in an evaporation chamber at a pressure of 10^{-5} mbar, were used as targets.

V. DISCUSSION

The model developed in this work gives a comprehensive analytical description of the DE technique and allows better designs of high-resolution instruments. In addition, the model assists in the selection of spectrometer parameters for more accurate initial velocity measurements. An inspection of the equations derived in Sec. II leads to several conclusions.

As $\tau_c \propto \sqrt{m}$, the exact critical delay condition can be tuned solely for a given value of m. For this preselected value, the corresponding ion species sensitivity increases dramatically once the peak width tends to zero. The complete collapse of the peak width does not occur due to existence of time-focusing aberrations, i.e., divergence of dN/dT exists only for ions having the energy E_0 given by $\tau = \tau_c(E_0)$. Ions of the same species with $E > E_0$ produce peak folding over the right-hand side of the peak (higher TOF). For $\tau \gg \tau_c$, the peak spreads out up to $\tau = t_{G1}(\varepsilon_0, 0)$, when it freezes. The quantity $\Delta\tau$ starts to play an important role in this situation because the extraction field is ramping while the ions of interest are crossing the acceleration grid. It is also found, for usual values of acceleration voltages and for typical values of ε_0 and $\Delta\tau$, that $\tau_c + \Delta\tau/2$ is poorly sensitive on ε_0 and on $\Delta\tau$. The effect of ε_0 on τ_c is to increase it by a quantity (few ns in the simulation presented in Fig. 5) which is roughly E_0 independent. The physical reason for this effect is that the leakage field spreads the secondary ion package and a longer τ is necessary to increase the final kinetic energy difference between the fast and the slow ions. The derivative $dT/d\tau$, used in ν_0 determination, decreases (4% in this case) when ε_0 is introduced; therefore, the same correction should be applied on ν_0 if this technique is employed.

For long-TOF instruments (i.e., $R\sqrt{RL} \gg 2d_1$), the value of P_m is given by Eq. (17). Note that $P_m \alpha \varepsilon_1^{3/2} \alpha (\Delta U)^{3/2}$, so that a high mass resolution mass spectrometer must have large ε_1 or ΔU values. Also, one sees from Eqs. (14) and (3) that $\tau_c \propto \sqrt{m}/\varepsilon_1^2$; if the extraction field ε_1 is too weak for a given m, then τ_c becomes of the order of t_{G1} and the resolving power cannot be increased sensibly. On the other hand, if ε_1 is too strong, sparking may occur and/or the critical delay may be too short to be easily implemented for measurements.

The present experiment was performed at laser fluences of about 1 J/cm^2, above the threshold of plasma formation. Analysis of experimental data is focused on the Cs^+ peak, the dominant peak in a TOF mass spectrum of a CsI sample.

Figure 8(b) shows that; as predicted by the simulations; the Cs^+ peak becomes narrower and higher with the increment of τ. It goes through a minimum width for $\tau = 278$ ns—a value close to τ_c—and tends to be very broad for $\tau > \tau_c$.

The broad distributions observed, as the delay time is increased, are the signature of the complex phenomena that occur during the ablation of CsI. The differences between the predicted shapes [Fig. 8(a)] and the observed ones [Fig. 8(b)] are very difficult to explain based on a one-component initial energy distribution. Two-component distributions are frequently reported in papers of laser ablation,[12,13,18,19] but the sources of these distributions are often a matter of discussion, due to the diversity of conditions in which laser ablation can occur. For the conditions of the present experiments, delayed emission of ions from the solid and hydrodynamics effects within the laser plume are among the most probable mechanisms that contribute to the observed peak shapes. A further analysis of the velocity distributions of the ejecta is mandatory to obtain a better understanding of this issue; in particular, effects on peak TOF due to laser intensity and gas phase collision inside the expanding plume are treated in Ref. 20.

APPENDIX

The basic equations of linear TOF spectrometers are briefly reviewed. The ion dynamics, from the target ($z = 0$) to the detector ($z = z_{\text{det}}$), are treated in one dimension. This means that only the axial component of the initial velocity (ν_0) is considered and electric fields are assumed to be perpendicular to the target.

The general expression for the ion TOF is

$$T = \int_0^{z_{\text{det}}} \frac{dz}{\nu}, \tag{A1}$$

where $\nu(z)$ is the ion velocity at the abscissa z. If the spectrometer electric field ε depends on both time and position, then Newton's second law has to be solved for an ion of charge q and mass m:

$$m \frac{d^2 z}{dt^2} = q\varepsilon(t,z). \tag{A2}$$

For linear spectrometers having several regions with uniform electric fields, Eq. (A2) may be solved region by region. Defining $d_n = z_n - z_{n-1}$ as the region width and $\Delta U_n = U_n - U_{n-1}$ as the potential difference for the nth region, this gives

$$\varepsilon_n(t) = \frac{\Delta U_n(t)}{d_n}, \tag{A3}$$

and the total TOF is the sum of the TOFs, t_n, relative to each region:

$$T=\sum_n t_n .$$

If in the nth region ε is not time dependent, the kinetic energy theorem gives for an ion located at z inside this region:

$$\frac{1}{2}m\nu^2-\frac{1}{2}m\nu_{n-1}^2=q\int_{z_{n-1}}^{z}\varepsilon(z)dz, \tag{A4}$$

which yields

$$\nu^2=\nu_{n-1}^2+\frac{2q}{m}(U-U_{n-1}). \tag{A5}$$

On the other hand, if uniform time-dependent fields exist, Eq. (A3) holds, $\nu(t)$ and $z(t)$ are calculated by integrating Eq. (A2) and t_n is determined.

This technique, called[1,8] is often employed in three-region spectrometers for initial velocity analyses.[10–14] It consists of keeping a null electric field in the first region for a time interval τ after the sample is ionized and then ramping the external field in a time interval $\Delta\tau$ up to a constant value. This can be done by varying the sample potential $U_0(t)$ while the first- and second-grid potentials (U_1 and U_2) are kept constant. The axial ion velocity inside the $n=1$ region is given by

$$\nu(t)=\nu_0+\frac{q}{md_1}\int_0^1(U_0(t)-U_1)dt, \tag{A6}$$

in which ν_0 is axial component of the initial velocity and d_1 is the distance from the sample to the first-acceleration grid. The TOF t_1 corresponding to this region is obtained by solving the integral of $\nu(t)$ given by Eq. (A7):

$$d_1=\int_0^{t_1}\nu(t)dt. \tag{A7}$$

Equations (A5) and (A7) are employed for the second and third regions in order to get the times t_2 and t_3. By summing the three t_n's, T is determined.

ACKNOWLEDGMENTS

This work was partially supported by the Brazilian agency CNPq and by FAPERJ. Two of the authors (V. M. C. and F. A. F.-L.) would like to respectively acknowledge the Proteomic Network of Rio de Janeiro and the Latin American Center of Physics (CLAF) for their scholarships.

[1] W. C. Wiley and I. H. McLaren, Rev. Sci. Instrum. **26**, 1150 (1955).
[2] J.-C. Tabet and R. J. Cotter, Int. J. Mass Spectrom. Ion Processes **54**, 151 (1983).
[3] S. M. Colby, T. B. King, and J. P. Reilly, Rapid Commun. Mass Spectrom. **8**, 865 (1994).
[4] R. S. Brown and J. J. Lennon, Anal. Chem. **67**, 1998 (1995).
[5] R. J. Cotter, *Time-of-Flight Mass Spectrometry: Instrumentation and Applications in Biological Research*, ACS Professional Reference Books (American Chemical Society, Washington, DC, 1997).
[6] M. Karas, J. Mass Spectrom. **32**, 1 (1997).
[7] D. C. Barbacci, R. D. Edmondson, and D. H. Russell, Int. J. Mass Spectrom. Ion Processes **165**, 221 (1997).
[8] M. L. Vestal and P. Juhasz, J. Am. Soc. Mass Spectrom. **9**, 892 (1998).
[9] P. Juhasz, M. L. Vestal, and S. A. Martin, J. Am. Soc. Mass Spectrom. **8**, 209 (1997).
[10] M. Glückmann and M. Karas, J. Mass Spectrom. **34**, 467 (1999).
[11] Y.-K. Choi, H.-S. Im, and K.-W. Jung, Int. J. Mass. Spectrom. **189**, 115 (1999).
[12] Y.-K. Choi, H.-S. Im, and K.-W. Jung, Appl. Surf. Sci. **150**, 152 (1999).
[13] S. Berkenkamp, C. Menzel, F. Hillenkamp, and K. Dreisewerd, J. Am. Soc. Mass Spectrom. **13**, 209 (2002).
[14] I. Fournier, A. Brunot, J. C. Tabet, and G. Bolbach, Int. J. Mass. Spectrom. **213**, 203 (2002).
[15] L. Schmidt, H. Juncglas, H.-W. Fritsch, and P. Köhl, *Proceedings of the 40th American Society for Mass Spectrometry (ASMS) Conference on Mass Spectrometry and Allied Topics* (ASMS, Washington, DC, 1992), p. 574.
[16] R. P. Schmid and C. Weickhardt, Int. J. Mass. Spectrom. **206**, 181 (2001).
[17] V. Montero Collado, Ph.D. dissertation, PUC-Rio, 2001.
[18] D. Geogehan, in *Pulsed Laser Deposition of Thin Films*, edited by D. B. Chrisey and G. K. Hubler (Wiley, New York, 1994), pp. 115–165.
[19] S. Georgiu and A. Koubenakis, Chem. Rev. (Washington, D.C.) **103**, 349 (2003).
[20] F. Fernández-Lima, V. M. Collado, C. R. Ponciano, L. S. Farenzena, E. Pedrero, and E. F. da Silveira, Appl. Surf. Sci. **217**, 202 (2003), and references therein.